Sustained State-Independent Quantum Contextual Correlations from a Single Ion

F. M. Leupold,[1] M. Malinowski,[1] C. Zhang,[1] V. Negnevitsky,[1] A. Cabello,[2] J. Alonso,[1*] and J. P. Home[1†]

[1]*Institute for Quantum Electronics, ETH Zürich, Otto-Stern-Weg 1, 8093 Zürich, Switzerland*
[2]*Departamento de Física Aplicada II, Universidad de Sevilla, 41012 Sevilla, Spain*

We use a single trapped-ion qutrit to demonstrate the quantum-state-independent violation of noncontextuality inequalities using a sequence of randomly chosen quantum nondemolition projective measurements. We concatenate 53×10^6 sequential measurements of 13 observables, and unambiguously violate an optimal noncontextual bound. We use the same data set to characterize imperfections including signaling and repeatability of the measurements. The experimental sequence was generated in real time with a quantum random number generator integrated into our control system to select the subsequent observable with a latency below 50 μs, which can be used to constrain contextual hidden-variable models that might describe our results. The state-recycling experimental procedure is resilient to noise and independent of the qutrit state, substantiating the fact that the contextual nature of quantum physics is connected to measurements and not necessarily to designated states. The use of extended sequences of quantum nondemolition measurements finds applications in the fields of sensing and quantum information.

Two measurements are said to be compatible when their outcome statistics for any given input state are indistinguishable from the individual statistics extracted from a joint measurement on that state. In classical theories, outcomes of measurements are consistent with each result having a preexisting value, independent of which other compatible measurements are performed. Quantum mechanics (QM) is bound by different rules, resulting in stronger correlations between the outcomes of compatible observables than are possible in classical theories. This feature, which is known as contextuality, has been linked to the power of quantum computation [1–4] and to reliable communication protocols [5,6], and its most famous manifestation is Bell nonlocality [7]. In this sense, the violation of a Bell inequality demonstrates contextuality. However, nonlocality requires composite systems in entangled states. A more general result is that of Kochen and Specker [8], who showed that any state of any quantum system in a Hilbert space of dimension greater than two can be used to reveal contextuality.

In a similar fashion to a Bell inequality, the contextuality of QM can be shown through the violation of a number of inequalities, which have been derived for systems of various Hilbert space dimension. Such inequalities can be split into those which are violated for a given input state [9,10] and those for which the violation is input-state independent [11,12]. State-independent-contextuality (SIC) tests have been performed using a number of systems [13–21], but thus far they all used the following approach: (i) prepare an input state and (ii) measure multiple observables. This was repeated for each of a finite number of input states, and using all combinations of observables required for the test. Measurements on each observable can be carried out either simultaneously or sequentially [22], with the sequential approach being the most popular.

An alternative proposal [23] is to perform a SIC test using sequences of ideal quantum nondemolition projective measurements (which in the context of general probabilistic theories are known as sharp measurements [24]). Each measurement is performed on the state into which the system was projected by the previous measurement. When executed in this manner, contextuality tests intrinsically sustain the generation of quantum correlations, which can be used to generate and certify continuous strings of random numbers [25,26].

In this Letter, we demonstrate SIC sustainable in time using state recycling over a sequence of 53×10^6 measurements. To that end we have adopted (i) the simplest system featuring SIC, a three-level quantum system or qutrit [8,27], (ii) the smallest set of elementary quantum measurements needed for SIC, namely, the Yu-Oh set with 13 observables [12,28,29], and (iii) the original Yu-Oh and an optimal witness of SIC [30]. Our results violate the bounds imposed by noncontextual hidden-variable models. We use a commercial quantum random number generator (QRNG) to create the sequence of measured observables in real time. This places constraints on contextual hidden-variable models attempting to explain our results, which must cover the behavior not only of the qutrit but also of the QRNG [31]. We quantify the unsharpness and incompatibility (or signaling, see
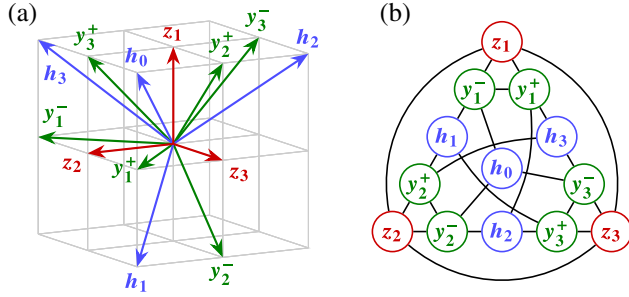
FIG. 1. Observables and compatibility relations between the observables for the Yu-Oh set. (a) The 13 rays are represented by vectors in a three-dimensional real Hilbert space. Their directional components are listed in Table I. (b) The orthogonality relationships between the rays determine a graph with 13 vertices and 24 edges between compatible rays.

Ref. [32]) of our measurements by extracting high-order correlators from the data set.

The 13 dichotomic ("yes-no") observables or "rays" in the Yu-Oh set [12] are of the form $A_v = I - 2P_v$, where I is the identity, P_v is the normalized projection operator onto a vector $|v\rangle = a|0\rangle + b|1\rangle + c|2\rangle$, and $\{|0\rangle, |1\rangle, |2\rangle\}$ form a qutrit basis. Since the eigenvalues of P_v are 0 and 1, ray measurements result in values $+1$ and -1. The 13 vectors $|v\rangle$ with real-valued coefficients (a, b, c) are defined by points on the surface of a cube in a three-dimensional Hilbert space [Fig. 1(a) and Table I]. Two rays are compatible if the corresponding vectors are orthogonal. This can be visualized in an orthogonality graph [Fig. 1(b)] by drawing all vectors from the set $V = \{y_k^\sigma, h_\alpha, z_k | k = 1, 2, 3; \sigma = \pm; \alpha = 0, 1, 2, 3\}$ as vertices and linking vertices of compatible rays. In this notation, z_k are the basis states, y_k are superpositions of two basis states, and h_k are superpositions of all three. In total, there are 24 edges in the graph, representing the 24 compatible pairs $(u, v) \in E$ with $P_u P_v = 0$ (each edge is counted only once).

Besides the original Yu-Oh witness [12],

$$\langle \chi_{\mathrm{YO}} \rangle = \sum_{v \in V} \langle A_v \rangle - \sum_{(u,v) \in E} \frac{1}{2} \langle A_u A_v \rangle, \qquad (1a)$$

we use the optimal SIC witness opt3 for which the QM and classical predictions differ maximally [30]:

$$\langle \chi_{\mathrm{opt3}} \rangle = \sum_{v \in V_h} 2\langle A_v \rangle + \sum_{v \in V \setminus V_h} \langle A_v \rangle$$
$$- \sum_{(u,v) \in E \setminus C_2} 2\langle A_u A_v \rangle - \sum_{(u,v) \in C_2} \langle A_u A_v \rangle$$
$$- \sum_{(u,v,w) \in C_3} 3\langle A_u A_v A_w \rangle. \qquad (1b)$$

TABLE I. Definition and experimental parameters for the vectors $v \in V$ in the Yu-Oh set. The coefficients (a, b, c) give the directions of the rays in the real-valued three-dimensional Hilbert space (Fig. 1). In the experiment, rays are rotated onto the measurement axis (along z_1) by applying the coherent rotations in Eqs. (4) using the angles $\theta_v^{(1)}, \phi_v^{(1)}, \theta_v^{(2)}, \phi_v^{(2)}$ (see also Fig. 3). The last column shows the corresponding bit sequence from the QRNG (see text for details). If the QRNG delivers a bit sequence not present in this table, it is discarded and a new one is read in. Shorthand notations $\bar{1} = -1$ and $\theta_h^{(2)} = 2\arctan(1/\sqrt{2})$ were used.

v	(a, b, c)	$\theta_v^{(1)}$	$\phi_v^{(1)}$	$\theta_v^{(2)}$	$\phi_v^{(2)}$	QRNG
y_1^-	$(0, 1, \bar{1})$	π	$3\pi/2$	$\pi/2$	$\pi/2$	0001
y_2^-	$(\bar{1}, 0, 1)$	0	0	$3\pi/2$	$3\pi/2$	0010
y_3^-	$(1, \bar{1}, 0)$	$\pi/2$	$\pi/2$	0	0	0011
y_1^+	$(0, 1, 1)$	π	$3\pi/2$	$\pi/2$	$3\pi/2$	0100
y_2^+	$(1, 0, 1)$	0	0	$\pi/2$	$3\pi/2$	0101
y_3^+	$(1, 1, 0)$	$\pi/2$	$3\pi/2$	0	0	0110
h_1	$(\bar{1}, 1, 1)$	$3\pi/2$	$3\pi/2$	$\theta_h^{(2)}$	$3\pi/2$	0111
h_2	$(1, \bar{1}, 1)$	$\pi/2$	$\pi/2$	$\theta_h^{(2)}$	$3\pi/2$	1000
h_3	$(1, 1, \bar{1})$	$\pi/2$	$3\pi/2$	$\theta_h^{(2)}$	$\pi/2$	1001
h_0	$(1, 1, 1)$	$\pi/2$	$3\pi/2$	$\theta_h^{(2)}$	$3\pi/2$	1010
z_1	$(1, 0, 0)$	0	0	0	0	1011
z_2	$(0, 1, 0)$	π	$3\pi/2$	0	0	1100
z_3	$(0, 0, 1)$	0	0	π	$3\pi/2$	1101

Here, $V_h = \{h_\alpha\}$, $C_2 = \{(z_k, y_k^+), (z_k, y_k^-), (y_k^+, y_k^-)\}$ and $C_3 = \{(z_k, y_k^+, y_k^-)\}$, with indices k and α running as for V. A necessary condition for a set of correlations to be noncontextual is

$$\langle \chi_{\mathrm{YO}} \rangle \le 8 \quad \text{and} \quad \langle \chi_{\mathrm{opt3}} \rangle \le 25, \qquad (2)$$

and any violation of these inequalities demonstrates contextuality. The prediction of quantum theory is that, for any qutrit state and under ideal conditions,

$$\langle \chi_{\mathrm{YO}} \rangle = \frac{25}{3} \approx 8.333 \quad \text{and} \quad \langle \chi_{\mathrm{opt3}} \rangle = \frac{83}{3} \approx 27.667. \qquad (3)$$

Our experimental platform to test these witnesses uses a single $^{40}\mathrm{Ca}^+$ ion confined in a surface-electrode radio frequency trap in the setup described in Ref. [43]. The qutrit basis states are represented by three fine-structure levels in a $^{40}\mathrm{Ca}^+$ ion: $|0\rangle = |S_{1/2}(m_j = -1/2)\rangle$ in the ground-state manifold, and $|1\rangle = |D_{5/2}(m_j = -3/2)\rangle$ and $|2\rangle = |D_{5/2}(m_j = -1/2)\rangle$ in the metastable $D_{5/2}$ manifold (Fig. 2). The two metastable states have a Zeeman-shifted energy difference $\hbar(\omega_2 - \omega_1) = (2\pi\hbar)6.47$ MHz in an external magnetic field of $B = 0.385$ mT.

Every experimental sequence starts with 500 μs of Doppler cooling using a 397 nm laser red detuned approximately half a natural linewidth from resonance
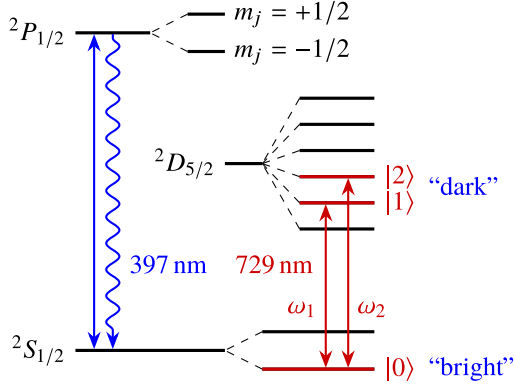
FIG. 2. Energy level diagram of the $^{40}\text{Ca}^+$ ion. Qutrit states $|0\rangle$, $|1\rangle$, and $|2\rangle$ are encoded in the highlighted fine-structure levels. Coherent rotations between them are achieved with laser pulses at 729 nm. Fluorescence measurements using an excitation laser at 397 nm project the qutrit state into either $|0\rangle$ ("bright") or the $|1\rangle,|2\rangle$ manifold ("dark").

with the cycling transition between the $S_{1/2}$ and $P_{1/2}$ manifolds, and with close to one saturation intensity [32,43]. This is followed by 10 μs of optical pumping to initialize the qutrit to the $|0\rangle$ state. Subsequently, measurements of the observables $\{A_v\}$ are performed, which consist of coherent rotations between the qutrit states and projective measurements. Coherent rotations are achieved using 729 nm laser pulses resonant with the transitions between $|0\rangle$ and $|1\rangle$ (at ω_1), and between $|0\rangle$ and $|2\rangle$ (at ω_2). Matrix representations of the rotations in the Hilbert space spanned by the basis $\{|0\rangle, |1\rangle, |2\rangle\}$ are given by

$$R^{(1)}(\theta,\phi) = \begin{pmatrix} \cos(\frac{\theta}{2}) & -ie^{-i\phi}\sin(\frac{\theta}{2}) & 0 \\ -ie^{i\phi}\sin(\frac{\theta}{2}) & \cos(\frac{\theta}{2}) & 0 \\ 0 & 0 & 1 \end{pmatrix}, \quad (4a)$$

$$R^{(2)}(\theta,\phi) = \begin{pmatrix} \cos(\frac{\theta}{2}) & 0 & -ie^{-i\phi}\sin(\frac{\theta}{2}) \\ 0 & 1 & 0 \\ -ie^{i\phi}\sin(\frac{\theta}{2}) & 0 & \cos(\frac{\theta}{2}) \end{pmatrix}. \quad (4b)$$

The angles θ and ϕ for a certain rotation (Table I) are controlled via the duration and phase of the corresponding laser pulse using an acousto-optic modulator. Projective measurements are realized by illuminating the ion for 160 μs with the same settings used for Doppler cooling [32]. If photons are scattered, the qutrit state is projected onto $|0\rangle$ ("bright state"), if not, the qutrit is projected onto the $D_{5/2}$ manifold ("dark states"), preserving the coherence between $|1\rangle$ and $|2\rangle$ (Fig. 2). For the bright (dark) states, we register on average 18.8 (0.7) photons through a high-numerical aperture objective on a photomultiplier tube. Thresholding single-shot photon counts at 5.5 for the 160 μs detection window allows us to distinguish bright from dark states with an estimated mean detection error of $< 2 \times 10^{-4}$ [32].

Testing the SIC inequalities on the Yu-Oh set [12] requires projective measurements along all 13 rays (Fig. 1). By design, the fluorescence detection projects onto either the qutrit state $|0\rangle$ itself, i.e., the z_1 ray, or the plane orthogonal to it, spanned by $|1\rangle$ and $|2\rangle$. For any other observable A_v, we apply first a unitary rotation $U_v = R^{(2)}(\theta_v^{(2)}, \phi_v^{(2)})R^{(1)}(\theta_v^{(1)}, \phi_v^{(1)})$, which rotates v onto z_1, then fluorescence detection (followed by optical pumping of the $S_{1/2}$ population to $|0\rangle$), and finally the reverse rotation $U_v^\dagger$ (Fig. 3). Every measurement of an observable is thus uniquely determined by v and is independent of the context.

Ideally, we would perform a single long series of measurements of randomly chosen observables. In practice, we interrupt the sequence to save collected data and periodically calibrate laser frequencies and pulse times. To sustain the sequence, we take subsequences containing a minimum of 1000 measurements, which we interrupt when the last detection projects the qutrit onto $|0\rangle$. The next subsequence then starts by initializing the qutrit to $|0\rangle$ and applying the rotation $U_{v_0}^\dagger$, with $v_0 = v_l$ the last ray from the previous sequence. In this way, all performed measurement sequences can be concatenated up to the 53×10^6 in the present data set [32]. The periodic reset resulting from the repeated measurements with a finite probability to find the system in $|0\rangle$ allows such long continuous sequences to
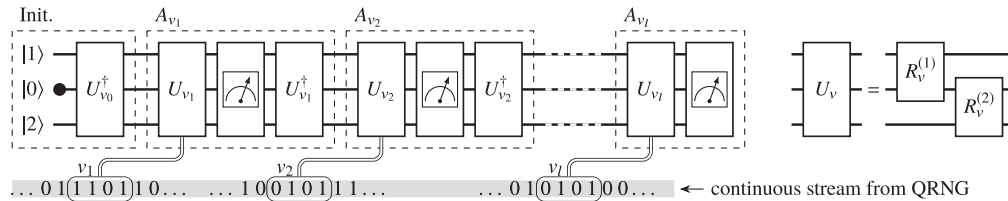

FIG. 3. Sequential measurement scheme. A subsequence starts by initializing the ion state to $|0\rangle$ and rotating it to the last ray from the previous subsequence, v_0. Every following ray measurement A_v then consists of a unitary transformation U_v rotating the ray v onto $|0\rangle$, a projective measurement, and the back rotation $U_v^\dagger$. The unitary transformations $U_v = R_v^{(2)}R_v^{(1)}$ are realized by coherent driving on the transitions between $|0\rangle$ and $|1\rangle$, $R_v^{(1)} = R^{(1)}(\theta_v^{(1)}, \phi_v^{(1)})$, and between $|0\rangle$ and $|2\rangle$, $R_v^{(2)} = R^{(2)}(\theta_v^{(2)}, \phi_v^{(2)})$. Subsequent measurement rays are determined by bit sequences from a QRNG, which are created after performing the respective previous projective measurement.

be built up while restricting the propagation of unitary-rotation errors.

We randomize the sequence of measured observables using a QRNG (model Quantis from ID Quantique SA). It delivers a constant stream of random bits, from which we take groups of four and assign rays v to them (Table I). The random bits for an observable are created after the detection event of the previous observable (Fig. 3). In this way, if we acknowledge the randomness of the QRNG, we prevent a hypothetically conspiring ion from knowing what the context of a measurement will be [31]. Everything from the QRNG output to the pulse sequence programmed in the computer-control system is updated in real time within a $50~\mu s$ time window between unitary rotations.

In a typical sequence of 10^6 measurements, we observe between two and five subsequences containing more than 55 dark measurements in a row. In a random sequence of 55 ideal measurements, we would, however, only expect such a set to occur with a probability of $(2/3)^{55} \approx 2 \times 10^{-10}$, which corresponds to a 1% probability for it to appear once in the full set of 53×10^6 measurements. We attribute this anomalous effect to off-resonant leakage into the states $|D_{5/2}, m_j = -5/2\rangle$ and $|D_{5/2}, m_j = +1/2\rangle$, which are long-lived dark states outside our computational Hilbert space [32]. The control system for the experiment spots these events in real time and breaks, purging the subsequence and starting a new subsequence from the same v_0 as was used for the purged subsequence.

Every data point measured for an observable A_v consists of the measurement ray v and an outcome $a = \pm 1$. From the full data set, we collect the numbers $N(A_v = a_1)$, $N(A_u = a_1, A_v = a_2)$, and $N(A_u = a_1, A_v = a_2, A_w = a_3)$, where A_u, A_v, and A_w are successive measurements in that order, for all $u, v, w \in V$ and all $a_1, a_2, a_3 \in \{1, -1\}$. Based on these numbers, we compute the expectation values,

$$\langle A_v \rangle = \frac{\sum_{a_1} a_1 N(A_v = a_1)}{\sum_{a_1} N(A_v = a_1)}, \tag{5a}$$

$$\langle A_u A_v \rangle = \frac{\sum'_{a_1,a_2} a_1 a_2 N(A_u = a_1, A_v = a_2)}{\sum'_{a_1,a_2} N(A_u = a_1, A_v = a_2)}, \tag{5b}$$

$$\langle A_u A_v A_w \rangle$$
$$= \frac{\sum'_{a_1,a_2,a_3} a_1 a_2 a_3 N(A_u = a_1, A_v = a_2, A_w = a_3)}{\sum'_{a_1,a_2,a_3} N(A_u = a_1, A_v = a_2, A_w = a_3)}, \tag{5c}$$

where $\sum'$ additionally sums over all permutations of the argument list of N, i.e., the measurement order. Substituting the obtained values (Fig. 4) into the SIC witnesses in Eqs. (1), we find

$$\langle \chi_{\mathrm{YO}} \rangle = 8.279(4) \quad \text{and} \quad \langle \chi_{\mathrm{opt3}} \rangle = 27.357(11). \tag{6}$$
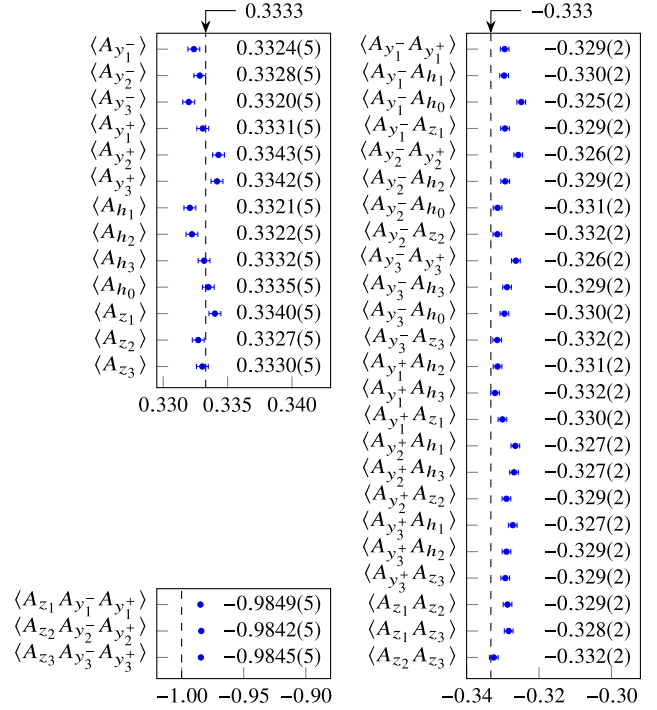

FIG. 4. Experimental results for expectation values that enter the SIC witnesses in Eqs. (1) (see text for details on their calculation). Error bars reflect shot noise, dashed lines represent values predicted by quantum mechanics.

	0.3333			−0.333
$\langle A_{y_1^-} \rangle$	0.3324(5)		$\langle A_{y_1^-} A_{y_1^+} \rangle$	−0.329(2)
$\langle A_{y_2^-} \rangle$	0.3328(5)		$\langle A_{y_1^-} A_{h_1} \rangle$	−0.330(2)
$\langle A_{y_3^-} \rangle$	0.3320(5)		$\langle A_{y_1^-} A_{h_0} \rangle$	−0.325(2)
$\langle A_{y_1^+} \rangle$	0.3331(5)		$\langle A_{y_1^-} A_{z_1} \rangle$	−0.329(2)
$\langle A_{y_2^+} \rangle$	0.3343(5)		$\langle A_{y_2^-} A_{y_2^+} \rangle$	−0.326(2)
$\langle A_{y_3^+} \rangle$	0.3342(5)		$\langle A_{y_2^-} A_{h_2} \rangle$	−0.329(2)
$\langle A_{h_1} \rangle$	0.3321(5)		$\langle A_{y_2^-} A_{h_0} \rangle$	−0.331(2)
$\langle A_{h_2} \rangle$	0.3322(5)		$\langle A_{y_2^-} A_{z_2} \rangle$	−0.332(2)
$\langle A_{h_3} \rangle$	0.3332(5)		$\langle A_{y_3^-} A_{y_3^+} \rangle$	−0.326(2)
$\langle A_{h_0} \rangle$	0.3335(5)		$\langle A_{y_3^-} A_{h_3} \rangle$	−0.329(2)
$\langle A_{z_1} \rangle$	0.3340(5)		$\langle A_{y_3^-} A_{h_0} \rangle$	−0.330(2)
$\langle A_{z_2} \rangle$	0.3327(5)		$\langle A_{y_3^-} A_{z_3} \rangle$	−0.332(2)
$\langle A_{z_3} \rangle$	0.3330(5)		$\langle A_{y_1^+} A_{h_2} \rangle$	−0.331(2)
0.330 0.335 0.340			$\langle A_{y_1^+} A_{h_3} \rangle$	−0.332(2)
			$\langle A_{y_1^+} A_{z_1} \rangle$	−0.330(2)
			$\langle A_{y_2^+} A_{h_1} \rangle$	−0.327(2)
			$\langle A_{y_2^+} A_{h_3} \rangle$	−0.327(2)
			$\langle A_{y_2^+} A_{z_2} \rangle$	−0.329(2)
			$\langle A_{y_3^+} A_{h_1} \rangle$	−0.327(2)
			$\langle A_{y_3^+} A_{h_2} \rangle$	−0.329(2)
			$\langle A_{y_3^+} A_{z_3} \rangle$	−0.329(2)
$\langle A_{z_1} A_{y_1^-} A_{y_1^+} \rangle$	−0.9849(5)		$\langle A_{z_1} A_{z_2} \rangle$	−0.329(2)
$\langle A_{z_2} A_{y_2^-} A_{y_2^+} \rangle$	−0.9842(5)		$\langle A_{z_1} A_{z_3} \rangle$	−0.328(2)
$\langle A_{z_3} A_{y_3^-} A_{y_3^+} \rangle$	−0.9845(5)		$\langle A_{z_2} A_{z_3} \rangle$	−0.332(2)
−1.00 −0.95 −0.90			−0.34 −0.32 −0.30	

Our results violate inequalities Eq. (2) by 69 and 214 standard deviations, which correspond to a contextual fraction of 0.167 and 0.177, respectively, out of a maximum of 0.2 in both cases [4,32]. These deviations are solely based on statistical uncertainties, which are small due to the large number of measurements in the complete data set. However, we believe that the significance of these violations should be penalized according to experimental imperfections and systematic errors [32], and elaborate on this issue below.

Our data set additionally allows for evaluation of the SIC witnesses in Eqs. (2) based on the "standard approach," where measurements are repeatedly performed on specifically prepared states of the system. For this, we calculate the averages conditioned on a preceding projection onto one of the states $i \in V$. We do this for all 13 input states and observe violations of the SIC inequalities by at least 15 and 43 standard deviations, respectively [32].

The inequalities in Eq. (2) are satisfied by any theory assuming noncontextuality and their violation indicates contextuality if certain underlying assumptions are satisfied. There are some such assumptions that are untestable, e.g., the assumption that observers have free will for choosing which measurement to make at any time (here implemented with a QRNG). Nevertheless, there are underlying assumptions that are (at least partially) testable. One is the assumption that measurements are sharp; i.e.,

they are minimally disturbing [24] and their outcomes are the same if performed repeatedly. In quantum theory, sharp measurements are represented by self-adjoint operators; the "ideal measurements" as defined by von Neumann [44] are sharp measurements. While perfect sharpness can never be fulfilled in a real experiment, we find the repeatability of our measurements (including rotations and projections) to be above 99.6% [32]. Another assumption is compatibility between the 24 pairs of observables in E [Fig. 1(b)]. Given compatibility, there should be (i) no context signaling in the data and (ii) no influence of preceding compatible measurements on the statistics of an observable [32]. The large number of measurements comprising our data set renders statistical uncertainties very small and we are able to resolve small systematic deviations from the ideal case in both these measures. We believe these should reflect on our results for the SIC witnesses [Eqs. (1)], but we are not aware of any standard method to account for these imperfections when evaluating SIC witnesses. There exist analytical methods to take into account such imperfections for noncontextuality inequalities for scenarios with cyclic systems in which dichotomic observables are measured in only two contexts [45]. These or other contextuality-by-default techniques [46] may serve as a starting point to account for imperfections also in the Yu-Oh scenario.

We characterize in Ref. [32] the quantum-versus-classical advantage of this experiment based on the fact that QM predictions for this system cannot be simulated with a classical trit, as this would require a classical system with a substantially larger memory. Furthermore, we show that the compatibility structure between observables need not be assumed *a priori*, but can be inferred from the resulting statistics without invoking QM.

Beyond addressing fundamental aspects of QM, this work demonstrates a system capable of autonomously generating quantum operations, a feature desirable for a prospective quantum computer. The system concatenates hundreds of millions of coherent rotations and projective measurements, rather than repeating a finite sequence which starts with a predefined quantum state and consumes a resource at the end of the computation. Such long sequences of quantum nondemolition measurements are interesting in a range of areas including sensing and quantum computing [47]. Furthermore, the methods presented in this Letter might be generalized to multiparticle quantum systems, providing more powerful tests of fundamental physics [48–50] and addressing the question of how to optimally generate, certify, and make use of quantum contextual correlations.

Experimental data were taken by F. M. L., M. M., and J. A., using an apparatus primarily built by F. M. L. and J. A., and with significant contributions from M. M., C. Z., and V. N. Data analysis was performed by F. M. L., J. A., J. P. H., and A. C. The paper was written by F. M. L., J. A., A. C., and J. P. H., with input from all authors. Experiments were conceived by A. C., F. M. L., J. A., and J. P. H. The authors declare that they have no competing financial interests.

[*]alonso@phys.ethz.ch
[†]jhome@phys.ethz.ch
[1] R. Raussendorf, Phys. Rev. A **88**, 022322 (2013).
[2] M. Howard, J. Wallman, V. Veitch, and J. Emerson, Nature (London) **510**, 351 (2014).
[3] J. Bermejo-Vega, N. Delfosse, D. E. Browne, C. Okay, and R. Raussendorf, Phys. Rev. Lett. **119**, 120505 (2017).
[4] S. Abramsky, R. S. Barbosa, and S. Mansfield, Phys. Rev. Lett. **119**, 050504 (2017).
[5] A. Cabello, V. D'Ambrosio, E. Nagali, and F. Sciarrino, Phys. Rev. A **84**, 030302 (2011).
[6] T. S. Cubitt, D. Leung, W. Matthews, and A. Winter, Phys. Rev. Lett. **104**, 230503 (2010).
[7] J. S. Bell, Physics **1**, 195 (1964).
[8] S. Kochen and E. P. Specker, J. Math. Mech. **17**, 59 (1967).
[9] J. F. Clauser, M. A. Horne, A. Shimony, and R. A. Holt, Phys. Rev. Lett. **23**, 880 (1969).
[10] A. A. Klyachko, M. A. Can, S. Binicioğlu, and A. S. Shumovsky, Phys. Rev. Lett. **101**, 020403 (2008).

[11] A. Cabello, Phys. Rev. Lett. **101**, 210401 (2008).
[12] S. Yu and C. H. Oh, Phys. Rev. Lett. **108**, 030402 (2012).
[13] G. Kirchmair, F. Zähringer, R. Gerritsma, M. Kleinmann, O. Gühne, A. Cabello, R. Blatt, and C. F. Roos, Nature (London) **460**, 494 (2009).
[14] E. Amselem, M. Rådmark, M. Bourennane, and A. Cabello, Phys. Rev. Lett. **103**, 160405 (2009).
[15] O. Moussa, C. A. Ryan, D. G. Cory, and R. Laflamme, Phys. Rev. Lett. **104**, 160501 (2010).
[16] C. Zu, Y.-X. Wang, D.-L. Deng, X.-Y. Chang, K. Liu, P.-Y. Hou, H.-X. Yang, and L.-M. Duan, Phys. Rev. Lett. **109**, 150401 (2012).
[17] X. Zhang, M. Um, J. Zhang, S. An, Y. Wang, D.-l. Deng, C. Shen, L.-M. Duan, and K. Kim, Phys. Rev. Lett. **110**, 070401 (2013).
[18] V. D'Ambrosio, I. Herbauts, E. Amselem, E. Nagali, M. Bourennane, F. Sciarrino, and A. Cabello, Phys. Rev. X **3**, 011012 (2013).
[19] Y.-F. Huang, M. Li, D.-Y. Cao, C. Zhang, Y.-S. Zhang, B.-H. Liu, C.-F. Li, and G.-C. Guo, Phys. Rev. A **87**, 052133 (2013).
[20] G. Cañas, S. Etcheverry, E. S. Gómez, C. Saavedra, G. B. Xavier, G. Lima, and A. Cabello, Phys. Rev. A **90**, 012119 (2014).
[21] G. Cañas, M. Arias, S. Etcheverry, E. S. Gómez, A. Cabello, G. B. Xavier, and G. Lima, Phys. Rev. Lett. **113**, 090404 (2014).
[22] O. Gühne, M. Kleinmann, A. Cabello, J.-A. Larsson, G. Kirchmair, F. Zähringer, R. Gerritsma, and C. F. Roos, Phys. Rev. A **81**, 022121 (2010).
[23] M. Wajs, S.-Y. Lee, P. Kurzyński, and D. Kaszlikowski, Phys. Rev. A **93**, 052104 (2016).
[24] G. Chiribella and X. Yuan, arXiv:1404.3348v2.
[25] R. Colbeck, Ph.D. thesis, University of Cambridge, 2007.
[26] M. Um, X. Zhang, J. Zhang, Y. Wang, S. Yangchao, D.-L. Deng, L.-M. Duan, and K. Kim, Sci. Rep. **3**, 1627 (2013).
[27] J. S. Bell, Rev. Mod. Phys. **38**, 447 (1966).
[28] A. Cabello, M. Kleinmann, and C. Budroni, Phys. Rev. Lett. **114**, 250402 (2015).
[29] A. Cabello, M. Kleinmann, and J. R. Portillo, J. Phys. A **49**, 38LT01 (2016).
[30] M. Kleinmann, C. Budroni, J.-Å. Larsson, O. Gühne, and A. Cabello, Phys. Rev. Lett. **109**, 250402 (2012).
[31] A. Peres and A. Ron, in *Microphysical Reality and Quantum Formalism*, Vol. 2, edited by A. V. der Merwe, F. Selleri, and G. Tarozzi (Kluwer, Dordrecht, 1985), pp. 115–123.
[32] See Supplemental Material at http://link.aps.org/supplemental/10.1103/PhysRevLett.120.180401, which includes Refs. [24,33–42], for further details.
[33] W. M. Itano, J. C. Bergquist, J. J. Bollinger, J. M. Gilligan, D. J. Heinzen, F. L. Moore, M. G. Raizen, and D. J. Wineland, Phys. Rev. A **47**, 3554 (1993).
[34] A. Cabello, Phys. Rev. A **93**, 032102 (2016).
[35] F. M. Leupold, Ph.D. thesis, ETH Zurich, 2015.
[36] A. Bermudez, X. Xu, R. Nigmatullin, J. O'Gorman, V. Negnevitsky, P. Schindler, T. Monz, U. Poschinger, C. Hempel, J. Home, F. Schmidt-Kaler, M. Biercuk, R. Blatt, S. Benjamin, and M. Müller, Phys. Rev. X **7**, 041061 (2017).
[37] D. Leibfried, R. Blatt, C. Monroe, and D. Wineland, Rev. Mod. Phys. **75**, 281 (2003).
[38] A. H. Myerson, D. J. Szwer, S. C. Webster, D. T. C. Allcock, M. J. Curtis, G. Imreh, J. A. Sherman, D. N. Stacey, A. M. Steane, and D. M. Lucas, Phys. Rev. Lett. **100**, 200502 (2008).
[39] M. Kleinmann, O. Gühne, J. R. Portillo, J.-Å. Larsson, and A. Cabello, New J. Phys. **13**, 113011 (2011).
[40] A. Cabello, M. Gu, O. Gühne, and Z.-P. Xu, Phys. Rev. Lett. **120**, 130401 (2018).
[41] A. Peres, Phys. Lett. A **151**, 107 (1990).
[42] N. D. Mermin, Phys. Rev. Lett. **65**, 1838 (1990).
[43] J. Alonso, F. M. Leupold, Z. U. Solèr, M. Fadel, M. Marinelli, B. C. Keitch, V. Negnevitsky, and J. P. Home, Nat. Commun. **7**, 11243 (2016).
[44] J. Neumann, *Mathematische Grundlagen der Quantenmechanik* (Springer, Berlin, 1932).
[45] J. V. Kujala, E. N. Dzhafarov, and J.-Å. Larsson, Phys. Rev. Lett. **115**, 150401 (2015).
[46] E. N. Dzhafarov, J. V. Kujala, and V. H. Cervantes, in *Quantum Interaction*, edited by H. Atmanspacher, T. Filk, and E. Pothos (Springer International Publishing, Cham, 2016), pp. 12–23.
[47] S. Haroche, Rev. Mod. Phys. **85**, 1083 (2013).
[48] A. Cabello, E. Amselem, K. Blanchfield, M. Bourennane, and I. Bengtsson, Phys. Rev. A **85**, 032108 (2012).
[49] X. Zhan, X. Zhang, J. Li, Y. Zhang, B. C. Sanders, and P. Xue, Phys. Rev. Lett. **116**, 090401 (2016).
[50] S. Abramsky, R. S. Barbosa, N. de Silva, and O. Zapata, arXiv:1705.07310.

Correction: The author order was presented incorrectly and has been fixed.